LIQUEFACTION OF THE BRAIN FOLLOWING STROKE SHARES MULTIPLE CHARACTERISTICS WITH ATHEROSCLEROSIS AND MEDIATES SECONDARY NEURODEGENRATION IN AN OSTEOPONTIN-DEPENDENT MECHANISM

by

Amanda Chung

A Thesis Submitted to the Faculty of the

DEPARTMENT OF CELLULAR AND MOLECULAR MEDICINE

In Partial Fulfillment of the Requirements

For the Degree of

MASTER OF SCIENCE

In the Graduate College

THE UNIVERSITY OF ARIZONA

2018

STATEMENT BY AUTHOR

The thesis titled *Liquefaction of the brain following stroke shares multiple characteristics with atherosclerosis and mediates secondary neurodegeneration in an osteopontin-dependent mechanism* prepared by *Amanda Chung* has been submitted in partial fulfillment of requirements for a master's degree at the University of Arizona and is deposited in the University Library to be made available to borrowers under rules of the Library.

Brief quotations from this thesis are allowable without special permission, provided that an accurate acknowledgement of the source is made. Requests for permission for extended quotation from or reproduction of this manuscript in whole or in part may be granted by the head of the major department or the Dean of the Graduate College when in his or her judgment the proposed use of the material is in the interests of scholarship. In all other instances, however, permission must be obtained from the author.

SIGNED: *Amanda Chung*

APPROVAL BY THESIS DIRECTOR

This thesis has been approved on the date shown below:

Kristian Doyle
Assistant Professor, Department of Immunobiology

4/18/18
Date

ACKNOWLEDGEMENTS

The author is infinitely grateful to Dr. Kristian P. Doyle for his mentorship and support during her time in the lab. She would also like to thank members of the Doyle lab: Dr. Thuy-Vi Vivian Nguyen, Jacob C. Zbesko, Jennifer Frye, and Megan Hayes for their continued help and support. The author also acknowledges Dr. Brian S. McKay, Anna G. Figueroa, Dr. John P. Konhilas, Eleni Constantopoulos, and W. Antony Day for their collaboration and technical assistance in this study. She is also thankful for the guidance of Dr. Lonnie Lybarger and Dr. Clark Lantz throughout this project.

TABLE OF CONTENTS

ABSTRACT

The response to ischemic injury in the brain is different to the response to ischemic injury in other organs and tissues. Almost exclusive to the brain, and for unknown reasons, dead tissue liquefies in response to ischemia by the process of liquefactive necrosis. However, the data we present here indicate that at the macroscopic, microscopic, and molecular level, liquefactive necrosis strongly resembles atherosclerosis. We show that chronic stroke infarcts contain foamy macrophages, cholesterol crystals, high levels of osteopontin and matrix metalloproteases, and a similar cytokine profile to atherosclerosis. Crystalline cholesterol is a principal driver of atherosclerosis, and because cholesterol is an important structural component of myelin, we propose that liquefactive necrosis in response to stroke is caused by an inflammatory response to myelin debris, and is exacerbated by the formation of cholesterol crystals within macrophages. We propose that this leads to the chronic production of high levels of proteases, which in a partially osteopontin-dependent mechanism, causes secondary neurodegeneration and encephalomalacia of the surrounding tissue. In support of this, we show that genetically ablating osteopontin substantially reduces the production of degradative enzymes following stroke, reduces secondary neurodegeneration, and improves recovery. These findings suggest that treatments that prevent or target the regression of atherosclerosis may also be useful for mitigating the harmful effects of liquefactive necrosis following stroke.

INTRODUCTION

Stroke is currently the fifth leading cause of death and a leading cause of long-term disability in the United States. Approximately 800,000 individuals have a stroke every year and nearly a quarter of these stroke cases occur in people who have previously experienced a stroke [1]. More than one third of stroke survivors will develop dementia within five years of having their stroke, and many more will live with long-term disabilities [2,3].

Ischemic strokes account for approximately 87% of all stroke cases. Ischemia occurs when blood flow to the brain is obstructed, often by a clot. Consequently, surrounding tissue cannot receive sufficient oxygen and nutrients. This can result in cellular death via excitotoxicity, ion imbalance, oxidative and nitrative stress, and inflammation [1,4]. As few as five minutes of ischemia and hypoxia can cause neuronal death [5]. Hemorrhagic strokes, characterized by rupture of a blood vessel in the brain, account for the remainder of stroke cases. Following hemorrhagic stroke, secondary damage occurs via cytotoxicity, excitotoxicity, oxidative stress, and inflammation [6].

Cellular death in response to ischemia

The initial insult of hypoxia due to ischemia results in a dramatic decrease in oxygen and glucose levels in the affected tissue, leading to an imbalance in cellular homeostasis. Oxidative phosphorylation, the main cellular pathway that produces ATP, requires oxygen as the last electron acceptor in the electron transport chain to produce a hydrogen gradient. Loss of the hydrogen gradient due to hypoxia will stall ATP synthesis, and the cell's ATP levels will drop dramatically. Na^+/K^+-ATPase pumps, which utilize a large pool of the ATP produced by oxidative phosphorylation, will not be able to function, resulting in a buildup of sodium and water within the cell and potassium in the extracellular space. The loss of an ion gradient results in

depolarization of neurons. If oxygen is not restored to the tissue, cells begin to swell, and the plasma membrane will begin to break [7]. Ultimately, cell death occurs and the cellular contents spill into the surrounding tissue. When molecules normally confined within the cell are released, toll-like receptors (TLRs) will recognize these molecules as damage-associated molecular patterns (DAMPs), consequently leading to an inflammatory response in the ischemic tissue [8]. Some of the cellular contents that leak from the infarct core can also cause excitotoxicity to the surrounding tissue, which can further exacerbate the injury.

Another form of cell death, apoptosis, also occurs in the hours and days following cerebral ischemia. This occurs more predominantly in the peri-infarct region because it is farther away from the infarct core and therefore has not been directly affected by ischemia, but has still been exposed to the toxins of the infarcted area [9–11,4]. Some mechanisms that promote apoptosis include damaged DNA, ATP in the extracellular space, reactive oxygen species, and free radicals, and the release of proapoptotic molecules from the mitochondria, such as cytochrome c, among others [11]. This mechanism of programmed cell death does not elicit the same inflammatory response as necrosis, but still contributes to neurodegeneration and cellular loss following stroke. Therefore, targeting mechanisms to minimize apoptosis of the ischemic penumbra can provide a useful therapeutic.

Tissue recovery following ischemia

Ischemic tissue undergoes sterile inflammation, which is an inflammatory response that occurs in the absence of infection. Sterile inflammation occurs in conditions such as stroke, atherosclerosis, particle-induced lung disease, and crystal-induced arthritis. There are a multitude of triggers of sterile inflammation, including intracellular molecules (nuclear proteins, mitochondrial DNA and peptides, *etc.*), extracellular matrix components, and cholesterol [12].

After the initial ischemic event in the brain, continued cell death occurs within the infarct and in the penumbra due to inflammation. An acute surge of leukocytes, including neutrophils, monocytes, and lymphocytes, to the infarcted area occurs 30 minutes to 24 hours following stroke [13]. Neutrophils are the first responders that migrate into the injured area via extravasation from the circulating blood. Their job in innate immunity is to phagocytose foreign material and debris and recruit additional immune cells by secreting cytokines and chemokines. Neutrophils can cause cellular damage via release of free radicals, cytokines, and proteolytic enzymes. They can also obstruct microcirculation during recruitment, further heightening tissue damage [13,14]. Lymphocytes, which are normally excluded from the central nervous system, migrate to the infarct approximately 24 hours post-stroke due to disruption of the blood brain barrier (BBB). Once there, they persist for weeks following stroke [15]. They play both beneficial and detrimental roles to the recovery of stroke. Lymphocytes promote glial scarring, which acts to isolate the ischemic core from surrounding tissue [14]. They can also produce a large amount of cytokines, chemokines, and antibodies that cause additional damage to the tissue.

In response to ischemia, tissue will undergo different forms of necrosis depending on the tissue and injury type. The brain is unique in that, in response to ischemia, it undergoes liquefactive necrosis rather than coagulative necrosis, which is more common in tissues such as the heart and kidney [7]. Liquefactive necrosis is also seen with infections or an intense inflammatory response. It is characterized by the transformation of normal tissue into a viscous mass due to the presence of proteinases and other enzymes that degrade the tissue. Microscopically, tissue architecture is lost and inflammatory cell debris is seen during liquefactive necrosis [7]. In the brain, liquefactive necrosis is a chronic inflammatory response to stroke that intensifies post-stroke injury [15–17] that occurs for unknown reasons. The final stage of

recovery is cystic encephalomalacia [17]. This is characterized by cystic cavities filled predominantly with cerebrospinal fluid, and the tissue that remains is softer than normal.

In the C57Bl/6 mouse model, the infarcted area is impacted by inflammation for approximately two weeks, at which time inflammation declines and a glial scar begins to form. This acts to separate the infarcted tissue from the surrounding tissue [14]. By seven weeks, the glial scar has matured but cytokine and chemokine levels are still elevated, indicating that the wound is still not fully healed [16]. Compared to the acute timeline of stroke recovery, the chronic progression of stroke recovery is not as well defined, with some sources stating that strokes resolve as early as 2 weeks, to other sources showing a continued pro-inflammatory profile in the lesion up to 14 weeks following stroke [7,17]. It is currently unknown why the inflammatory response continues for so long. Thus, it is imperative to study the multitude of factors that can contribute to the prolonged inflammatory response following stroke in order to provide better treatments for stroke patients.

Atherosclerosis and stroke

Cholesterol is a driving force for the progression of atherosclerosis. Atherosclerotic plaques develop within arteries when macrophages ingest excessive cholesterol in the form of oxidized low-density lipoprotein (oxLDL) [18]. Macrophages slowly develop into large proinflammatory foam cells that contain numerous lipid-laden cytoplasmic vesicles. The formation of foam cells is dictated by the balance between extracellular lipid uptake and reverse lipid transport from the intracellular compartment to extracellular lipid acceptors, such as high-density lipoprotein (HDL) and apolipoprotein E (apoE). If cholesterol accumulation within a foam cell exceeds the solubility limit of the cell, cholesterol crystals will form [18]. Intracellular cholesterol crystals can cause both physical damage to organelles by destabilization of the

lysosomal compartment and rupturing the plasma membrane [19] They can also activate the Nod-like receptor family pyrin domain containing 3 (NLRP3) inflammasome and the Syk and PI3 kinase pathway, resulting in the production of proinflammatory cytokines and degradative enzymes [18,20,21]. Extracellular cholesterol crystals can also activate the foreign body response, which likewise leads to the production of degradative enzymes [22,23].

Oxidized LDL also initiates pro-inflammatory Toll-like receptor 4 (TLR4) signaling through a complex composed of CD36, TLR4, and TLR6 [24]. The net effect of the convergence of inflammasome and TLR signaling is activation of nuclear factor-κB (NF-κB). This leads to T-lymphocyte recruitment, the production of reactive oxygen species (ROS) and reactive nitrogen species (RNS), and the production of proinflammatory cytokines [21] and degradative enzymes [20]. Therefore the goal of this study was to test if this mechanism that causes atheromas in cardiovascular disease is also the reason why dead brain tissue liquefies following stroke due to the fact that the brain is the most cholesterol-rich organ, containing approximately 20% of the body's total cholesterol [25].

In support of this hypothesis, Cantuti-Castelvetri et al recently demonstrated that in a toxin-induced model of demyelination, myelin debris can overwhelm the efflux capacity of microglia/macrophages, resulting in the formation of cholesterol crystals and a chronic inflammatory response in aged mice [26]. Furthermore, transcriptional profiling of macrophages at 7 days after spinal cord injury reveals that they closely resemble foam cells, with lipid catabolism representing their main biological process [27].

Molecular targets to decrease cytotoxic environment of liquefactive necrosis

To further elucidate similarities between atherosclerosis and stroke, we aimed to test if targeting pathways involved in the pathophysiology of atherosclerosis also modulate the damaging effects of liquefactive necrosis following stroke. The molecules we selected to target are osteopontin (OPN), CD36, and NLRP3.

Osteopontin

OPN is a secreted extracellular matrix protein that is involved in many processes, such as tissue repair, remodeling, and inflammation [28]. In inflammation, OPN acts as a proinflammatory or chemotactic cytokine [28,29]. OPN is one of the most abundant cytokines found in atherosclerotic lesions and it is involved in macrophage retention at sites of chronic inflammation [29]. OPN is also known to regulate chronic inflammatory responses to foreign bodies such as cholesterol crystals as evidenced by the fact that there are deficits in macrophage accumulation in OPN deficient mice in models of atherosclerosis and biomaterial implantation [29]. Bruemmer et al showed that OPN-deficient mice had slower progression of atherosclerotic lesions compared to their wildtype counterparts [30]. For these reasons, we chose to test if knocking out OPN would speed up recovery following stroke.

CD36 and NLRP3

CD36 and NLRP3 are both involved in the production of pro-inflammatory cytokines in atherosclerotic lesions and contribute to the progression of atherosclerosis. CD36 is a pathogen recognition receptor (PRR), specifically a scavenger receptor expressed on various cell types, including monocytes, macrophages, and endothelial cells. Macrophage CD36 is involved in atheroma formation by binding to oxidized low-density lipoprotein (oxLDL), thereby facilitating the formation of foam cells [31]. One specific signal cascade that is activated in response to

uptake of oxLDL by CD36 is the NLRP3 inflammasome. If the amount of oxLDL exceeds its solubility limit within lysosomal compartments, it precipitates into cholesterol crystals [18]. This crystallization destabilizes the lysosomal compartment, and a second signal is produced to induce inflammasome activation [32]. Once activated, the NLRP3 inflammasome leads to the secretion of IL-1 and IL-18. The NLRP3 inflammasome can also become activated in response to extracellular cholesterol crystals found in atherosclerotic lesions [18]. Genetic ablation of both CD36 and NLRP3 have been shown to reduce atherosclerotic lesion formation and progression [18,32].

Study objectives

The three main objectives of this thesis were 1) to compare the kinetics and characteristics of the inflammatory response to ischemia in the heart, a protein rich organ, to the inflammatory response to ischemia in the brain, a cholesterol rich organ, 2) to provide evidence of overlap in the molecular profile of the chronic inflammatory response to stroke and atherosclerosis, and 3) to test if targeting pathways involved in the pathophysiology of atherosclerosis also modulate the damaging effects of liquefactive necrosis following stroke.

Summary of Findings

We show that the brain takes substantially longer than the heart to heal from ischemia, with the induction of a second wave of inflammation that coincides with the formation of intracellular and extracellular cholesterol crystals within the infarct in the weeks following stroke. This second wave of inflammation could further aggravate and prolong the healing process. The second wave notably includes the expression of many of the same pro-inflammatory cytokines and proteolytic enzymes associated with atherosclerosis. We then show that the expression of these pro-inflammatory cytokines and proteolytic enzymes is profoundly reduced in OPN-

deficient mice, which correlates with an accelerated recovery of motor function and reduction in secondary neurodegeneration compared to wildtype mice. Surprisingly, we did not find a similar phenotype in CD36- or NLRP3- deficient mice. Nevertheless, these findings provide a compelling explanation for why the brain liquefies following stroke. Namely, that cholesterol derived from myelin debris overwhelms the processing capability of phagocytic cells in the brain, leading to the overproduction of degradative enzymes, and secondary neurodegeneration in an OPN dependent mechanism. Importantly, they are also a starting point for testing if treatments that target atherosclerosis and the chronic production of degradative enzymes are also useful for mitigating the damaging effects of liquefactive necrosis in recovering stroke patients.

MATERIALS AND METHODS

Mice

Adult 10-12 week male C57Bl/6J (Stock No: 000664), BALB/c (Stock No: 000651), NLRP3 knockout (Stock No: 021302), CD36 knockout (Stock No: 019006), and OPN knockout mice (Stock No: 025378) were purchased from the Jackson Laboratory (Bay Harbor, ME). All animals were housed under a 12-h light/dark schedule with *ad libitum* access to food and water. All animal manipulations were performed in accordance with National Institutes of Health guidelines and the University of Arizona IACUC procedures.

Stroke surgeries

C57BL/6 mice, NLRP3 KO mice, CD36 KO mice, and OPN KO mice underwent distal middle cerebral artery occlusion (DMCAO) on the mice as described previously in [33]. Briefly, mice were anesthetized by isoflurane inhalation core body temperature was maintained at 37ºC, and the skull exposed by creating an incision in the skin and temporalis muscle. The right middle cerebral artery (MCA) was identified and a microdrill was used to penetrate the skull to expose the underlying MCA. The meninges were cut and the vessel cauterized using a small vessel cauterizer (Bovie Medical Corporation). Surgical wounds were closed using Surgi-lock 2oc (Meridian Animal Health). Mice were then immediately transferred to a hypoxia chamber containing 9% oxygen and 91% nitrogen for 45 minutes. Sham surgeries were performed identically to stroke surgeries, except for cauterization of the DMCA. BALB/c mice underwent DMCAO without hypoxia. All mice received one dose of buprenorphine (0.1 mg/kg) via subcutaneous injection prior to surgery. Cefazolin antibiotics (25 mg/kg) and slow-release buprenorphine (1 mg/kg) were subcutaneously administered immediately following surgery.

Myocardial infarction

C57BL/6 mice were placed in the supine position, and a light was shone onto the neck region for transesophageal illumination, enabling the larynx to be visualized through the mouth opening. The tongue was retracted and a guide wire is inserted into the trachea. A 20G IV catheter was then laced over the guide wire and advanced into the trachea but not past the trachea bifurcation. The intubation tubing was then connected to the rodent ventilator. A left thoracotomy was then performed by a left lateral incision and transection of the third rib using dissecting scissors. An 8-0 polyethylene suture was threaded underneath the left coronary artery, perpendicular to the long axis of the heart. The ligature was tied and blanching of the myocardium was visually verified. The thoracotomy was closed in 3 layers: (1) the intercostal ribs and muscle, (2) the pectoral muscle and (3) the skin layers using 7-0 nylon absorbable suture. After each surgery was complete, the expiration line of ventilator was briefly occluded in order to evacuate the pleural space and establish proper intrapleural pressure. Mice were extubated and recovered on a heating pad. Total time under anesthesia: < 30 minutes.

Tissue processing

C57BL/6 mice were euthanized 24 hours, 1 week, 4 weeks, 8 weeks, and 6 months after stroke by deep isoflurane anesthesia followed by intracardial perfusion with 0.9% saline. BALB/c, NLRP3 knockout, CD36 knockout, and OPN knockout mice were euthanized at 7 weeks following stroke by the same methods. Brains and hearts were extracted and either snap frozen in liquid nitrogen for biochemical assays or fixed in 4% PFA and transferred to 30% sucrose for cryoprotection for immunohistochemistry, or placed in 2.5% glutaraldehyde and 2% PFA for electron microscopy. Coronal sections were obtained using a Microm HM 450 sliding microtome (Thermo Fisher Scientific) and stored in cryoprotectant solution containing 30% sucrose at -20º C.

Immunohistochemistry

Immunostaining was performed on free-floating 40 μm coronal brain sections and 6 μm coronal heart sections using standard techniques. Primary antibodies against neuronal nuclei (NeuN; 1:500; Millipore Sigma, Cat. No. MAB377, RRID: AB2298772), CD3e (1:1000; BD Biosciences, Cat. No. 550277, RRID: AB393573), CD68 (1:1000; Bio-Rad, Cat. No. MCA1957GA RRID: AB324217), and B220 (1:500; BD Biosciences, Cat. No. 553085, RRID: AB394615) were used in conjunction with the appropriate secondary antibody and ABC Vector Elite and 3,3'-diaminobenzidine kits (Vector Laboratories). Samples were visualized under light microscopy using a Keyence BZ-X700 microscope.

Nissl staining

Brain and heart sections were mounted and dehydrated. Slides were then cleared in xylene, rehydrated, immersed in 0.5% cresyl violet acetate (Sigma-Aldrich) solution for 1 minute, rinsed with distilled water, and differentiated in 0.25% acetic alcohol. Slides were then dehydrated through a graded ethanol series, cleared by xylene, and coverslipped using Entellan (Electron Microscopy Sciences). Samples were visualized under light microscopy using a Keyence BZ-X700 microscope.

Trichrome staining

Trichrome staining was performed on both 40 μm coronal brain sections and 6 μm coronal heart sections to determine formation of a collagen network in the infarcted tissue. Staining was performed according to AbCam trichrome stain (ab150686) protocol. Briefly, the heart sections were deparaffinized and hydrated to distilled water and brain sections were mounted and hydrated to distilled water. Bouin's fluid was preheated in a water bath to 56-64º C in a fume hood and slides were incubated in Bouin's fluid for 1 hour followed by 10 minutes of

cooling. The slides were rinsed in tap water for 5 minutes and rinsed once in distilled water. Slides were stained with Weigert's Iron Hematoxylin for 5 minutes and rinsed in running tap water for 2 minutes. Slides were placed in Briebirch Scarlet/Acid Fuchin solution for 15 minutes and subsequently rinsed in distilled water. Slides were then differentiated in Phosphomolybdic/Phosphotungstic acid solution for 10-15 minutes followed by application of Aniline Blue solution for another 5-10 minutes and rinsed in distilled water. Acetic acid solution (1%) was applied to the slides for 3-5 minutes, followed by dehydration in 95% alcohol twice and absolute alcohol twice. Finally, slides were cleared in xylene and mounted in Entellan.

Multiplex immunoassay

Snap-frozen brain tissue samples were sonicated in ice-cold 0.1 M PBS containing 1% triton-X and 0.1% sodium deoxycholate, Protease Inhibitor Cocktail (1:100; Millipore Sigma), and Phosphatase Inhibitor Cocktail 2 (1:100; Millipore Sigma). Following centrifugation, the total protein concentration of each supernatant was measured using a Direct Detect Infrared Spectrometer (Millipore Sigma). Total matrix metalloproteinases (MMPs), osteopontin (OPN), and cytokines and chemokines were then quantified using mouse multiplex magnetic bead kits purchased from Millipore Sigma, and used according to the manufacturer's recommendations. Each lysate sample, standard, and quality control was measured in duplicate. Plates were read using a MAGPIX instrument (Luminex), and results were analyzed using MILLIPLEX Analyst 5.1 software (Millipore Sigma).

Electron microscopy

Brains used for transmission and scanning electron microscopy (EM) were fixed in 2.5% glutaraldehyde + 2% PFA in 0.1 M Pipes buffer for 1 hour at room temperature or overnight at 4^{o}C. Following washes in 0.05 M Pipes buffer/0.05 M glycine and washes in 0.1 M Pipes buffer,

dissected stroke regions from each brain were then post-fixed in 1% osmium tetroxide for 1 hour. After fixation, samples underwent washes in deionized water (DIW). Samples for transmission EM were then block stained in 2% aqueous uranyl acetate, washed in DIW, dehydrated through a graded series of alcohols, infiltrated with 1:1 alcohol/Spurr's resin overnight, and embedded in 100% Spurr's resin overnight at 60^{o}C. Samples for scanning EM were dehydrated, incubated in hexamethyldisilazan, and then air dried. Sections for transmission EM were viewed under an FEI Tecnai Spirit microscope (Arizona Health Science Center Core Imaging Facility) operated at 100 kV. Eight-bit TIFF images were captured using an AMT 4 Mpixel camera. Sections for scanning EM were gold coated, and viewed under a FEI Company Inspect S microscope operated at 30 kV.

Cholesterol crystal imaging

Slides were prepared by washing 40 μm coronal brain sections in 1x PBS for 5 minutes three times. The sections were then mounted and dried on a slide warmer at 40º C for 1 hour, or until completely dried. Slides were washed three times in ddH_2O for two minutes and dried on a slide warmer at 40º C for 1 hour. Slides were cover slipped using glycerol and the edges were sealed with clear nail polish. The cholesterol crystals in the infarct were visualized using polarized light microscopy. Two polarized filters, the polarizer and analyzer, were adapted onto a Keyence BZ-X700 microscope. The filters were adjusted until maximum extinction was achieved. Images of the infarct that contained cholesterol crystals were captured using a 20x air objective. Lipofuscin autofluorescence was also captured as an overlay using a TexasRed filter cube (Keyence) to localize the lesion.

Cholesterol crystal isolation and verification

To confirm the presence of cholesterol crystals, sucrose density gradient centrifugation was performed to confirm that the crystals seen in the lesion have the same density as cholesterol crystals. Stroked mice were euthanized 7 weeks following DH stroke as described above. The infarct from C57BL/6 mice (n=5-10) were dissected and pooled. The same was performed with the equivalent area of contralateral cortex. Tissue was placed into two sterile 15 mL conical centrifuge tubes containing 750 μL of media (serum-free Neurobasal media, 1× B27 supplement, L-glutamine, and penicillin/streptomycin, without protease/phosphatase inhibitors; Thermo Fisher Scientific). Pooled tissue was gently triturated by passage through a sterile P1000 pipet. Dissociated cells were centrifuged at 300 rpm for 10 minutes at 4º C. The supernatant was removed, the pellet was re-suspended in 750 μL of fresh media followed by gentle trituration with a P1000 pipet, and the sample re-centrifuged at 300 rpm for 10 minutes at 4º C. Again, the supernatant was removed, the pellet was re-suspended in fresh media, and samples were stored at -80º C. Prior to pouring the sucrose density gradient, infarct samples were spun at 4,000 rpm for 15 minutes at 4º C. The supernatant was extracted and placed in a 2 mL screw cap micro tube. 1 mL of lysis buffer with added protease inhibitor and phosphatase inhibitors was added to the pellet and the sample was sonicated in bursts. Following sonication, samples were spun at 13,000 rpm for 15 minutes at 4º C. The supernatant was extracted and placed in a 2 mL screw cap micro tube and the pellet was resuspended in 200 μL of lysis buffer and triturated. This was repeated using the equivalent amount of the contralateral cortex. Each sample was poured into a linear sucrose gradient (0-2 M sucrose). Gradients were then centrifuged at 38,000 x *g* for 3 hours in an ultracentrifuge. Fractions were removed in 200 μL aliquots from the top of the gradient and analyzed for sucrose content with a refractometer. Using polarized microscopy, 10 μL of each fraction was placed onto a slide and the number of cholesterol crystals present in each fraction was counted. This experiment was repeated in triplicate.

Cholesterol assay

A cholesterol assay was also performed on the purified cholesterol crystal samples to validate that the crystals were cholesterol. Each fraction that we obtained from the sucrose density gradient centrifugation experiment was analyzed using the Amplex Red Cholesterol Assay Kit (Invitrogen). Briefly, samples were diluted in 1X reaction buffer and 50 μL of each sample was pipetted into separate wells of a microplate, along with controls. 50 μL of a solution of Amplex Red reagent, HRP, cholesterol oxidase, and cholesterol esterase was added to each well, followed by an incubation in the dark for 30 minutes at 37º C. Following incubation, fluorescence was measured using a fluorescent microplate reader using excitation between 530-560 nm and emission detection ~590 nm.

Ladder test

Ladder testing was performed on osteopontin wildtype and knockout mice to look at changes in motor recovery following stroke as described [34]. The test was performed at baseline, twice a week for the first 4 weeks post-surgery, and once a week between 5 and 7 weeks post-surgery. Mice were recorded from below with a handheld camcorder and the footage was analyzed frame-by-frame using standard film editing software (iMovie for Mac OSX 10.4). A correct step was defined as a limb placed on a rung without being removed. A missed step was defined as a limb placed between rungs. If a limb was placed on a rung and subsequently placed on the same rung again, this counted as two correct steps. If a limb was placed on a rung and subsequently slipped off the rung, a correct step and incorrect step were both recorded. Percent error was calculated as: 100 x [missed step/(missed + correct + correction step)].

Quantification of neuronal degeneration

Neurodegeneration in osteopontin deficient mice was measured by quantifying changes in percent area stained by NeuN in the peri-infarct striatum. NIH Image J analysis software was used to perform global thresholding in conjunction with a watershed algorithm on both the ipsilateral and equivalent location on the contralateral striatum. The peri-infarct striatum was measured at bregma 0.02 (n=5-6 per experimental group). Data was presented as ratio of percentage stained by NeuN in the ipsilateral/contralateral hemisphere.

Statistical analysis

Multiplex immunoassays were performed with blinding to experimental condition. However, blinding was not possible for immunostaining experiments because of the infarct being visible in stroked mice. Data are expressed as mean $\pm$ standard error of the mean (SEM). Statistical analyses were performed with Prism 6.0 software (GraphPad), with the level of significance set at $p < 0.05$. For multiplex immunoassay experiments, differences in protein concentrations in experiments with two experimental groups were analyzed by a Student's t-test. Differences in protein concentrations in experiments with three or more experimental groups were analyzed by one-way ANOVA. NeuN immunohistochemistry and cholesterol crystal data were analyzed using one-way ANOVA.

RESULTS

The brain heals much slower compared to the heart following ischemia

The brain is unique in that it undergoes liquefactive necrosis following ischemia, whereas the heart and other tissues will undergo coagulative necrosis following ischemia [7]. We have previously demonstrated that the liquefactive brain is imperfectly segregated form infarcted brain tissue by glial scars, and this liquefactive state intensifies post-stroke injury in the weeks following stroke [15]. The reason why the brain undergoes liquefactive necrosis in response to ischemia, and why the infarct remains in a liquefactive state for weeks following stroke is unknown. Therefore, in order to improve our understanding of why the brain responds to ischemia by liquefactive necrosis rather than coagulative necrosis, we first compared the kinetics and characteristics of the inflammatory response to ischemia in both the brain and the heart. Mice underwent experimentally induced stroke or myocardial infarction and were sacrificed 24 hours, 1 week, 4 weeks, and 8 weeks later (**Fig 1A**). Tissue was processed for either multiplex immunoassay or immunohistochemistry.

Cresyl violet acetate (Nissl) staining showed that each model of ischemia produced a large infarct of comparable size, and as expected, there was extensive tissue remodeling in both organs in the weeks following ischemia (**Fig 1B**). The brain is edematous 24 hours post-stroke compared to a naïve brain. Swelling is attenuated at 1 week, and by 4 weeks, the ipsilateral hemisphere begins to atrophy. By 8 weeks, atrophy is still present and ventricular enlargement is notable. Comparatively, the infarcted tissue in the heart begins to atrophy as early as 1 week following myocardial infarction, at which time ventricle enlargement is also present **(Fig 1B)**.

There is a similar cytokine response in infarcted brain and heart acutely. However, there was a considerable divergence in the chronic inflammatory response. In both tissues, the initial cytokine response subsided within 4 weeks. There were no significant changes in the cytokine expression in the heart at 8 weeks. In the brain, a second wave of pro-inflammatory cytokine expression appeared between weeks 4 and 8. This was evidenced by a significant increase in the levels of IP-10, KC, MCP-1, MIP-1α, MIP-1β, MIP-2, RANTES, IL-9, IL-4, and IL-12(p70) within the infarct at 8 weeks post stroke compared to naïve brain tissue (**Fig 1C**).

Furthermore, although there was substantial immune cell infiltration in both the brain and heart at 1 week following ischemia, by 4 weeks following ischemia, there was a clear discrepancy in the amount of immune cell infiltration and fibrosis present within each type of infarct (**Fig 1D**). In comparison to the brain, the heart infarcts contained markedly more collagen and substantially fewer T-lymphocytes, B-lymphocytes, and CD68+ macrophages at 4 weeks following ischemia. This difference was also evident at 8 weeks following ischemia (**Fig 1E**). There was also no apparent reduction in immune cell infiltration or any apparent increase in collagen deposition in the brain infarcts between 4 weeks and 8 weeks following ischemia. These data indicate that liquefaction of the brain following stroke correlates with a second wave of cytokine expression, scant collagen deposition, and more extensive chronic immune cell infiltration than occurs in the heart following a myocardial infarction.

In order to understand why the second wave of cytokine expression develops in the infarct in the weeks following stroke, and why the chronic immune cell infiltrate is more substantial and sustained, we looked closely at the configuration of cytokines that were significantly elevated at the 8-week time point. This revealed a molecular fingerprint reminiscent of the cytokine profile present in atheroma. Specifically, IP-10, KC, MCP-1, MIP-1α, MIP-1β,

MIP-2, RANTES, IL-9, IL-4, and IL-12(p70) have all been found in atherosclerotic plaques [35,36] Significantly, blocking IP-10 and MCP-1 results in atherosclerosis regression in mice [35]. Our previous data demonstrate that the human brain at the stage of liquefactive necrosis also contains increased levels of IP-10, MCP-1, MIP-1α, MIP-1β, and IL12(p70) [17]. Therefore, liquefaction of the brain following stroke shares several cytokine characteristics with atherosclerosis.

Characterization of liquefactive necrosis

Following stroke, infarcted tissue will undergo liquefactive necrosis, which is a unique response to hypoxia that occurs in the brain [37]. More typically, infarcted tissue undergoes coagulative necrosis, as seen in the heart. Coagulative necrosis occurs when hypoxia leads to an imbalance in the cell resulting in protein denaturation and cell death. In contrast, liquefactive necrosis is characterized by the enzymatic degradation of cellular debris and surrounding tissue by digestive enzymes that have been released from injured cells or inflammatory cells [37].

In light of this overlap in the cytokine profile between liquefactive necrosis of the brain following stroke and atherosclerosis, we hypothesized that the sustained state of liquefactive necrosis in response to stroke may be due to cholesterol crystal formation within macrophages that engulf cholesterol-rich myelin debris. Therefore, we evaluated the macroscopic (**Fig 2A**) and microscopic (**Fig 2B-C**) features of liquefactive necrosis and looked for the presence of cholesterol crystals (**Fig 2D-I**). As expected, scanning electron microscopy revealed that liquefactive necrosis is predominantly comprised of a sea of foamy macrophages, also known as gitter cells, that closely resemble foam cells, which are found predominantly in atherosclerotic lesions (**Fig 2B-C**). Transmission electron microscopy revealed that each macrophage contains an abundance of lipid droplets (**Fig 2D**). Importantly, transmission

electron microscopy also provided evidence that many of these macrophages contain cholesterol crystals, as evident by the clefts in the cytoplasm (**Fig 2E**). These findings of lipid droplets and cholesterol crystals within macrophages in the brain infarct further show the similarities between the cellular and molecular characteristics of atherosclerotic lesions and liquefactive necrosis following stroke.

Cholesterol crystals are birefringent and change the polarization of transmitted light [38]. Therefore, to validate that macrophages in areas of liquefactive necrosis indeed contain cholesterol crystals, we imaged the 24 hour, 1 week, 4 week and 8 week-old stroke infarcts using polarized light microscopy. This revealed that birefringent crystals appear within stroke infarcts between weeks 1 and 4 following stroke, and are even more abundant at 8 weeks following stroke (**Fig 2F-G**). This timeline of appearance of crystals correlates with the second wave of cytokine expression within the infarct and the failure of the immune cell infiltrate to resolve between 4 and 8 weeks following stroke.

Although transmission electron microscopy and polarized light microscopy are gold standard techniques for the identification of cholesterol crystals [38], we further tested if these crystals were comprised of cholesterol by performing sucrose density gradient centrifugation. Cholesterol crystals have a reported density of 1.04 g/ml [39]. Crystals isolated from cells extracted from areas of liquefactive necrosis 7 weeks following stroke had heterogeneous needle-like and plate-like morphologies, which matches the physical description of cholesterol crystals [39] (**Fig 2H**), and they had densities that ranged between 1.030-1.059g/ml, thus closely matching the reported density of cholesterol crystals (**Fig 2I**). These experiments provide evidence that chronic liquefactive necrosis of the brain in response to stroke is associated with the accumulation of cholesterol crystals within macrophages.

Shared characteristics between atherosclerosis and liquefactive necrosis

To determine if liquefaction of the brain following stroke shares other characteristics with atherosclerosis we measured the levels of osteopontin (OPN), IL-18, MMP-2, MMP-3, and MMP-8. OPN is one of the most abundant proteins present within atheroma and is expressed at high levels in other crystallopathies [40]. IL-18, a cytokine secreted following activation of the NLRP3 inflammasome complex, contributes to the progression of atherosclerosis [41]. Importantly, cholesterol crystals have been shown to activate the NLRP3 inflammasome in atheroma [18]. Furthermore, cholesterol crystals induce MMP expression in macrophages, and MMPs are abundant in atheroma [20,42]. We therefore chose to measure the levels of OPN, IL-18, MMP-2, MMP-3, and MMP-8 to further determine overlap between atherosclerosis and liquefactive necrosis. Multiplex immunoassay revealed that OPN is present at markedly high levels in areas of liquefactive necrosis 7 weeks following stroke (**Fig 3A**). IL-18 is also present (**Fig 3B**) and there are also strikingly high levels of MMP-2, MMP-3, and MMP-8 (**Fig 3C-E**) at up to 8 weeks following stroke compared to myocardial infarction. This chronic elevation of degradative enzymes indicates that could be continuous degradation of any matrix that may be laid down in the stroke lesion. This could account for the stark contrast between the collagen network in the heart and the sparse collagen present in the brain at 8 weeks following ischemia.

Cholesterol crystals and MMPs are present in the area of liquefactive necrosis in BALB/c mice

We next tested if the formation of cholesterol crystals and the high expression of MMPs in areas of liquefactive necrosis is specific to C57BL/6 mice, or specific to DH stroke. BALB/c mice underwent DMCAO without hypoxia and were sacrificed 7 weeks later. These mice also developed birefringent crystals in the infarct in the weeks after stroke (**Fig 4A**), and

had abundant expression of MMP-2, MMP-3, and MMP-8 (**Fig 4B**) in the area of liquefaction 7 weeks following stroke.

Liquefactive necrosis is resolved by 24 weeks

Our next step in characterizing the progression of stroke recovery was to determine how long it takes for liquefaction to resolve. Therefore, we stroked mice and euthanized them 6 months following stroke to assess for resolution of liquefactive necrosis. At 6 months following stroke, we observed a decrease in inflammatory cells (T-cells, macrophages, and B-cells) within the infarct **(Fig 5A)**. There was also a concomitant decrease in cytokine, chemokine, and MMP levels in the lesion 6 months post-stroke **(Fig 5B-C)**. This decrease in MMPs compared to the 8-week time point was concordant with the formation of collagen in the lesion. This suggests that a decrease in proteinase and collagenase levels at this time point allows for the formation of a collagen scar, similar to the collagen scar that is present in the heart at 8 weeks post-ischemia.

Targeting OPN attenuates the chronic inflammatory response following stroke

We then tested if targeting mediators that contribute to the pathophysiology of atherosclerosis using genetically modified mice could mitigate the production of cytokines and proteases within chronic stroke infarcts and improve stroke outcome. The three molecular targets were NLRP3 using NLRP3-deficient mice, CD36 using CD36-deficient mice, and OPN using OPN-deficient mice. NLRP3 is a key component of the inflammasome complex, which produces IL-1β and IL-18 once activated by crystalline structures [18]. We hypothesized that the genetic ablation of NLRP3 would prevent the activation of the NLRP3 inflammasome by cholesterol crystals. CD36 is a cell surface scavenger receptor involved in both cholesterol uptake by macrophages and NLRP3 inflammasome activation in atherosclerosis [24,31]. OPN

regulates macrophage chemotaxis [43] as well as production of MMPs by macrophages in atherosclerotic lesions [44] **(Fig 6A)**.

NLRP3-, CD36-, and OPN- deficient mice underwent DH stroke and were sacrificed 7 weeks later. The levels of cytokines and MMPs in the area of liquefaction were then analyzed by multiplex immunoassay and compared to wildtype mice. Levels of and IL-1β were significantly reduced in the NLRP3-deficient mice (**Fig 6B**), however other cytokine levels and MMP levels were unchanged (**Fig 6C**). There were no changes in cytokine or MMP levels in the CD36-deficient mice except for a reduction in TNF-α (**Fig 6B-C**). The biggest change in the levels of cytokines and MMP levels was evident in the OPN-deficient mice. G-CSF, IL-12(p70), IP-10, MCP-1, MIP-1α, MIP-1β, RANTES, TNF-α, MMP-2, and MMP-8 were all significantly and substantially reduced (**Fig 6B-C**).

Genetic ablation of OPN improves recovery and reduces secondary neurodegeneration

Based on the considerable reduction in cytokine and protease expression present in the area of liquefaction in the OPN-deficient mice, we next determined if this correlated with an improvement in recovery and a reduction in secondary neurodegeneration. We subjected the mice to a ladder rung test to examine motor recovery. Compared to wildtype mice, OPN-deficient mice recovered motor function significantly faster following DH stroke (**Fig 7A**) than wildtype mice. OPN-deficient mice also exhibited a greater preservation of neurons in the peri-infarct location as evinced by increased NeuN immunoreactivity (**Fig 7B-D**).

DISCUSSION

Using mouse models of ischemic stroke and myocardial infarction, we tested whether the brain takes longer to heal from an ischemic injury than the heart. We demonstrated that the inflammatory response to ischemic injury in the brain takes longer to resolve than the inflammatory response to ischemic injury in the heart. Indeed, in the brain there is a biphasic elevation of cytokines in the area of liquefactive necrosis, with the second phase initiated between weeks 4 and 8 after ischemic injury. This second phase coincided with the accumulation of intracellular and extracellular cholesterol crystals within the infarct.

This second wave of cytokines closely resembles the cytokine profile present in atherosclerotic plaques [36]. For example, there was significant elevation of the expression of MCP-1, IP10, and RANTES in the area of liquefactive necrosis. These cytokines are found to be upregulated in atheroma, and contribute to disease progression [45–48]. Our previous data demonstrate that the human brain at the stage of liquefactive necrosis contains many of the cytokines found in atheroma [17]. There is also a predominance of foamy macrophages and T-lymphocytes in the stroke infarct during the second elevation of cytokine expression, in common with the pathogenesis of atheroma.

Atherosclerosis progression is driven by macrophages that are unable to properly control cholesterol efflux, leading to the formation of foam cells [39]. Excessive cholesterol uptake can also result in the accumulation of free cholesterol in the lipid droplets, which can be toxic to cells. Free cholesterol that has deposited in cell membranes can create lipid rafts, which are denser than normal plasma membranes. The formation of lipid rafts in the membrane can further augment the inflammatory response by TLR signaling [21,27]. Furthermore, previous studies have shown that unresolved inflammation secondary to defective cholesterol efflux can

lead to a prolongation of the pro-inflammatory state, where macrophages are unable to switch from a pro-inflammatory to anti-inflammatory phenotype [49,50]. One moderator of a pro-inflammatory state in atherosclerosis is oxysterol, which is a product of cholesterol metabolism. Oxysterol is a derivative of cholesterol that is more polar and biochemically reactive, and is involved in both the expression and synthesis of pro-inflammatory cytokines in atherosclerotic lesions [51].

When the cholesterol concentration exceeds the solubility limit in foam cells, cholesterol crystals form within lysosomes [18,39]. Accumulation of cholesterol crystals can destabilize the lysosomal compartments, leading to the activation of the NLRP3 inflammasome. Activation of the NLRP3 inflammasome initiates a strong immune response in atherosclerosis by activating IL-1 and IL-18 [18]. Congruently, we found evidence of NLRP3 inflammasome activity within ischemic stroke infarcts during the chronic stage of liquefactive necrosis, as supported by a sustained elevation of IL-18 at 8 weeks following stroke. Comparatively, IL-18 was not detected to be elevated in the heart following myocardial infarction.

With regard to other cytokines found in the area of liquefactive necrosis, of the cytokines we analyzed, osteopontin was the most notably elevated. This molecule is unique in that it acts as both an immobilized extracellular matrix protein as well as a cytokine that is upregulated following myocardial infarction [42,52] . Osteopontin is one of the most abundant cytokines overexpressed in atheroma, is suggested to be an enhancer of atherosclerosis [29,52], and is also a key mediator in macrophage recruitment [53]. This provides another link between atherosclerosis and the area of liquefactive necrosis.

We also examined MMP expression given the known association of MMPs with atherosclerotic plaque. Under normal homeostatic conditions, MMPs are involved in developmental and physiological activities such as myelin formation, axonal growth, angiogenesis, and regeneration [54–56]. However, an abnormal ratio of MMP to their tissue inhibitors (TIMPs) in adult brains may contribute to pathologies such as Alzheimer's disease, ischemia, malignant glioma, and Parkinson's disease [55].

In the area of liquefactive necrosis, there was chronic and abundant expression of MMP-2, MMP-3, and MMP-8 following stroke compared to the equivalent area of infarction in the heart. Expression of MMP-2 was 100-fold higher (4,273 pg/mg), expression of MMP-3 was almost 3000-fold higher (15,059 pg/mg), and expression of MMP-8 was 500-fold higher (15,059 pg/mg) at 8 weeks post stroke compared to näive tissue. Interestingly, out of the total proteins we identified in this study, approximately 90% was comprised of MMPs. This chronically high expression of MMPs is a probable explanation for why the brain liquefies and remains liquefactive for months following stroke, and why brain infarcts present with less collagen deposition at 4 weeks and 8 weeks following ischemia when compared to the heart. MMPs can degrade myelin and so the initial high production of MMP-2, MMP-3, and MMP-8 at 24 hours following stroke likely occurs as a response to damaged myelin [57,58]. However, the overproduction of MMPs in the CNS is neurotoxic due to their capacity to disrupt tight junctions and degrade intact myelin on healthy neurons. Furthermore, MMP-2 converts stromal cell derived factor 1 (SDF-1), which is produced by reactive astrocytes, into a highly neurotoxic fragment [59–61]. Other degradative enzymes such as lipases are also likely to be substantially elevated in areas of liquefactive necrosis following stroke. The full characterization of this repertoire is likely to reveal important new targets for reducing secondary neurodegeneration.

Macrophages produce MMPs not only in response to damaged myelin, but also in response to cholesterol crystals [20]. This is surprising because MMPs target proteins rather than lipids. Nonetheless, Corr et al have shown that the treatment of primary macrophages with cholesterol crystals leads to crystal ingestion and activation of Syk and PI3K within minutes, followed by an over 500-fold increase in MMP-1 production. This may be because extracellular cholesterol crystals are able to activate the foreign body response. The foreign body response leads to the formation of multinucleated giant cells that generate large amounts of MMPs and other proteolytic enzymes [62,63]. Giant cells can engulf and digest large particles, or if the particles are too large for engulfment, they mediate bulk digestion via the extracellular release of degradative enzymes [23]. In the 1970s, Bayliss performed a time course study in which he demonstrated that giant cells can convert cholesterol crystals injected subcutaneously into Wistar rats into droplets of esterified cholesterol over a period of 3 months [22]. This provides a link between the presence of myelin debris and cholesterol crystals in chronic stroke infarcts, the sustained production of MMPs, and ultimately the clearance of cholesterol crystals and the resolution of liquefactive necrosis.

There is also a direct link between OPN and MMP expression. Extracellular matrix metalloproteinase inducer (EMMPRIN) is an upstream inducer of several MMPs and is a master regulator of MMP production [64]. OPN is linked to MMP production because the COOH-terminus of OPN, which is released upon thrombin cleavage and contains a cryptic SLAYGLR motif, is an EMMPRIN agonist. Specifically, the thrombin cleaved COOH-terminal fragment of OPN forms a complex with cyclophilin C, which upon engagement of EMMPRIN has been shown in murine mammary epithelial tumor cell lines to lead to phosphorylation of Akt and MMP-2 activation and secretion [44]. Cyclophilin C and cyclophilin-C-associated protein (CyCap) are expressed by macrophages in response to tissue damage [65] and in the brain, cyclophilin C complexes with

CyCap to activate microglia via the calcineurin/NFAT pathway [66]. We demonstrated that osteopontin deficient mice had a significant decrease in MMP expression in the stroke infarct. Osteopontin is a known substrate for several MMPs, including MMP-2, -3, -7, and -9 [67]. Elevation of osteopontin is also thought to drive MMP production via CD44 binding and the NF-kB pathway.

Further supporting the importance of OPN in the mechanism of liquefactive necrosis, OPN is known to regulate chronic inflammatory responses to foreign bodies such as cholesterol crystals as evidenced by the fact that there are deficits in macrophage accumulation in OPN-deficient mice in models of atherosclerosis and biomaterial implantation [29]. Furthermore, in response to exposure to calcium oxalate crystals, renal epithelial cells increase the production of OPN [40]. These data are interpreted as indicating that OPN is important in promoting the retention of macrophages at sites of chronic inflammation [29]. With regard to therapeutic intervention, G-CSF, IL-12, IP-10, MCP-1, MIP-1α, MIP-1β, RANTES, TNF-α, MMP-2, and MMP-8 were substantially reduced in OPN knock-out mice seven weeks following stroke, and these mice exhibited less secondary neurodegeneration in the peri-infarct location. These data suggest that OPN is a promising target for therapeutic intervention in chronic stroke.

Surprisingly, genetically ablating the NLRP3 inflammasome, which is activated by intracellular cholesterol crystals, had little impact on cytokine production or the MMP response to stroke. Although IL-1 levels were reduced in the area of liquefaction as expected, no other protein measured in this study was altered. This unexpected result suggests that the NLRP3 inflammasome may be less integral to the pathophysiology of liquefactive necrosis than OPN. A potential explanation for this result is that NLRP3 is not required for the full development of the foreign body response [68]. Therefore, a NLRP3-independent foreign body response to

extracellular cholesterol crystals may be a greater driver of chronic cytokine and degradative enzyme production following stroke than the activation of the NLRP3 inflammasome by intracellular cholesterol crystals.

An additional explanation is that there may be another consequence of myelin debris clearance other than the formation of cholesterol crystals that prevents the inflammatory response to stroke from resolving as efficiently as the inflammatory response to myocardial infarction. A possible example is the formation of oxysterols. Oxysterols are one of the products of cholesterol processing in foam cells and are a pro-inflammatory mediator in atherosclerotic lesions[51,69]. More research is needed to determine the relative contributions of myelin debris metabolites such as oxysterols, and cholesterol crystals, to the pathogenicity of liquefactive necrosis within chronic stroke infarcts. This should be prioritized because although it has yet to be fully characterized the extent to which humans form cholesterol crystals in the brain following stroke, in 1987 Miklossy and Van der Loos reported that crystals of cholesterol esters are present for at least 20 months in the human brain after stroke, both within the area of infarction, as well as the tracts originating in, and passing through the region of infarction [70,71].

Cholesterol esters and triglycerides are not present to a significant degree in the normal adult brain [72]. However, when macrophages and microglia are cultured with myelin, within 30 hours, 35% of the myelin cholesterol is converted to cholesterol esters and triglycerides and stored within lipid droplets [72]. CD36 is a key regulator of lipid droplet formation during atherogenesis due to its ability to bind to lipoproteins, oxidized phospholipids, fatty acids, and oxidized low density lipoprotein. However, the genetic ablation of CD36 had little impact on chronic cytokine production and MMP expression after stroke. This may be due to redundancy in scavenger receptor expression on the surface of microglia and macrophages. Nonetheless,

the targeting of alternative scavenger receptors and multiple scavenger receptors simultaneously should still be explored.

Concluding remarks and future directions

The similarities, revealed by this study, between atherosclerosis and liquefactive necrosis of the brain following stroke, provide new drug targets to mitigate the negative effects of the prolonged inflammatory response to stroke. For example, a pharmacological treatment that decreases the number of extracellular and intracellular cholesterol crystals that accumulate in chronic stroke infarcts could be a therapeutic strategy. One such treatment is to use the drug cyclodextrin. Cyclodextrin has been used to solubilize hydrophobic drugs to facilitate drug delivery. It has also been tested as a potential treatment for atherosclerosis as well as other CNS diseases such as Alzheimer's, multiple sclerosis, and spinal cord injuries [73,74]. Based on positive results from these studies there is a strong likelihood that cyclodextrin could reduce the cholesterol crystal burden in the area of liquefactive necrosis, and thereby lead to a better outcome in patients that have suffered a stroke. A future direction includes administering cyclodextrin to mice that have been subjected to a stroke to determine if cyclodextrin treatment lessens the cholesterol crystal burden following stroke. We will also test for behavioral changes, including motor recovery and cognition, as well as analyze secondary neurodegeneration to determine if cyclodextrin is a viable treatment.

In conclusion, a major function of lipids in myelin is to pack the membrane into a stable, long-lived insulating sheath. A consequence of this is that it is difficult to degrade, and the release of myelin following stroke appears to overwhelm the cholesterol degradation capacities of phagocytosing microglia and macrophages [75]. Thus, liquefaction of the brain following stroke shares multiple characteristics with atherosclerosis, the implication of which is that treatments

that target cholesterol loading within macrophages and the sustained production of degradative enzymes, such as neutralization of OPN, may help to prevent the damaging effects of liquefactive necrosis following stroke.

FIGURES

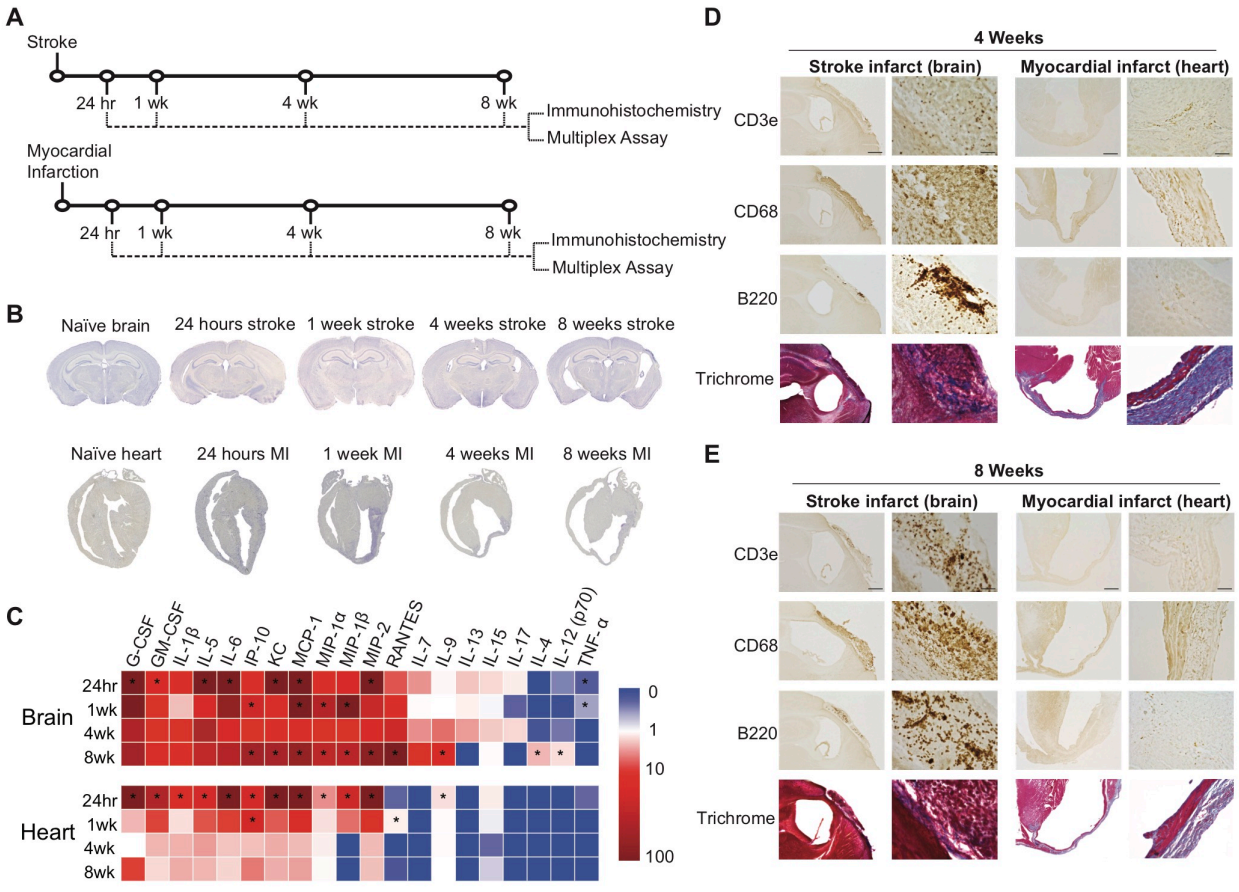

Fig. 1. The inflammatory response to ischemic injury is slower to resolve in the brain compared to the heart. (**A**) Experimental design. Mice were either given a stroke or myocardial infarction and were euthanized 24 hours, 1 week, 4 weeks, or 8 weeks following surgery. Infarcted tissue was dissected and processed for analysis by either immunohistochemistry or multiplex immunoassay. (**B**) Nissl staining demonstrates tissue morphology following the respective models of ischemia in the brain and heart. (**C**) Heat map of inflammatory marker expression detected by multiplex immunoassay in the brain and heart at 24 hours, 1 week, 4 weeks, and 8 weeks following ischemia. Values are expressed as fold change relative to naïve heart and brain controls. *p<0.05. (**D**) Comparison of immune cells present in the infarct in the brain and heart at 4 weeks following ischemic injury. There is more extensive infiltration of T-

lymphocytes (CD3e; top panel), microglia/macrophages (CD68; middle first panel), and B-lymphocytes (B220; middle second panel) in the brain compared to the heart. Conversely, there is a much more collagen deposition (blue staining; bottom panel) in the heart, compared to the brain. (**E**) Comparison of immune cells present in the infarct in the brain and heart at 8 weeks following ischemic injury. Scale bar, 500 μm for low (4x) magnification images, and 50 μm for high (20x) magnification images. n=5-7 mice per time point and assay. (1A-E courtesy of Jennifer Frye).

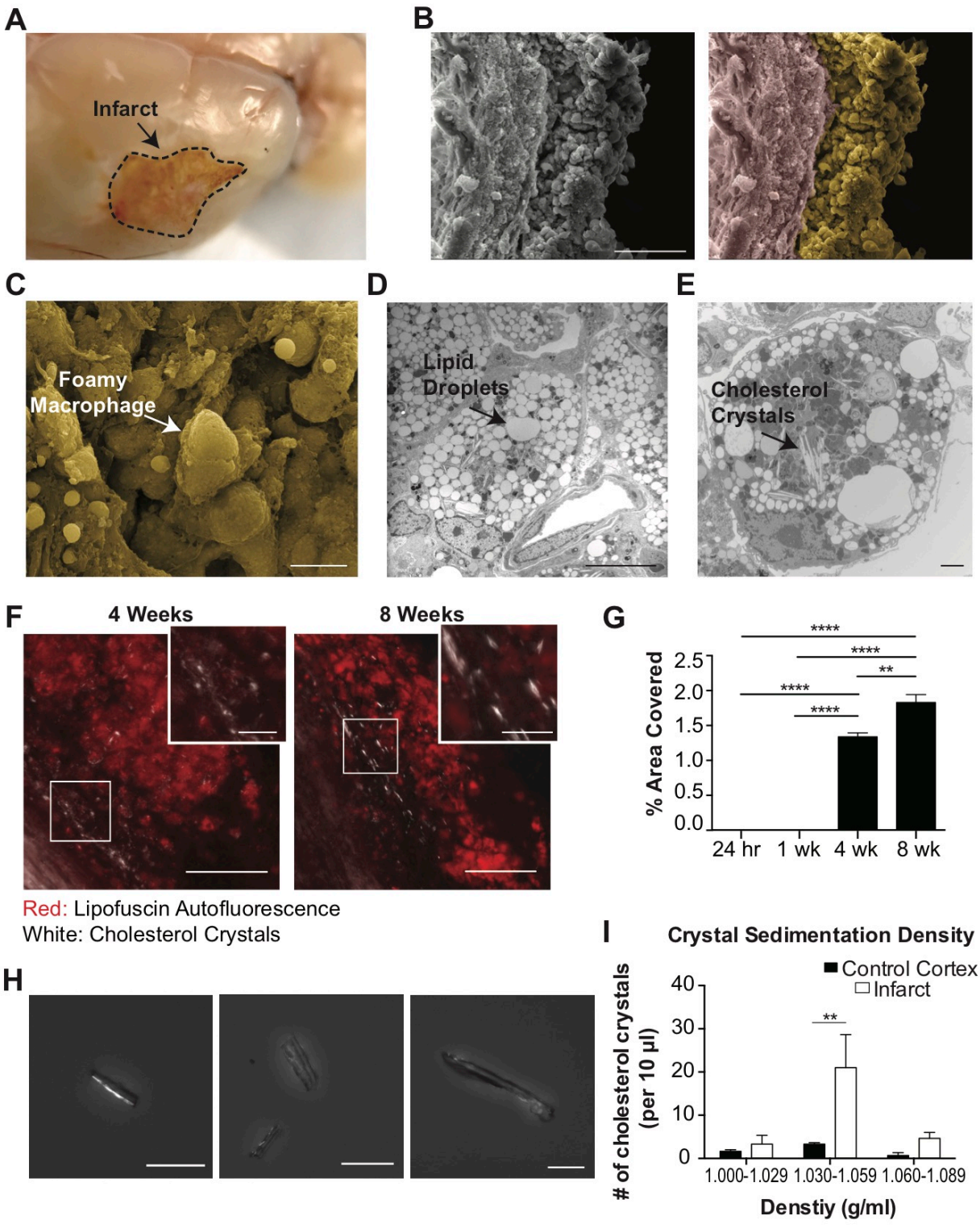

Fig. 2. Foamy macrophages within areas of liquefactive necrosis contain cholesterol crystals. (**A**) Gross pathology of a lesion (delineated) 7 weeks following stroke. The infarcted

area is in a liquefactive state. (**B**) Original (left image) scanning EM image of a 7-week infarct with a dense population of cells (pseudocolored yellow; right image) and glial scar (pseudocolored purple; right image). Scale bar, 100 μm. The infarct is filled with foamy macrophages (arrow), as seen magnified in (**C**). Scale bar, 50 μm. (**D**) Transmission EM of a macrophage in the infarct at 7 weeks following stroke. There is an accumulation of lipid droplets (arrow), providing the macrophage with its characteristic foamy appearance. Scale bar, 10 μm. (**E**) Transmission EM of a foamy macrophage in the infarct at 7 weeks following stroke with putative cholesterol crystal clefts in the cytoplasm (arrow). Scale bar, 2 μm. (**F**) Confirmation of the presence of extracellular cholesterol crystals (white) in the infarct by overlaying images taken with polarized and fluorescent microscopy. Lipofuscin autofluorescence (red) demarcates the area of infarction. Scale bar, 100 μm. Inset scale bars, 25 μm. (**G**) Quantification of cholesterol crystals in the lesion at 24 hours, 1 week, 4 weeks, and 8 weeks following stroke. Data represents mean ± SEM from n=4-5 mice per experimental group. **p<0.01 and **** p<0.0001. (**H**) Cholesterol crystals, purified from 7-week infarcted brains using sucrose density gradient centrifugation, and visualized under polarized microscopy. Cholesterol crystals were identified by the presence of light refraction. Scale bar, 50 μm. (**I**) The number of cholesterol crystals present in fractionated densities from chronic stroke infarcts or the equivalent area on the contralateral hemisphere (control cortex). Data represent mean ± SEM from n=3 sucrose density gradient centrifugation runs with n=5-10 mice per experiment. **p<0.01. (2A courtesy of Kristian P. Doyle, 2B-E courtesy of Antony Day, 2H-I data without analysis provided by Brian S. McKay and Anna Figueroa).

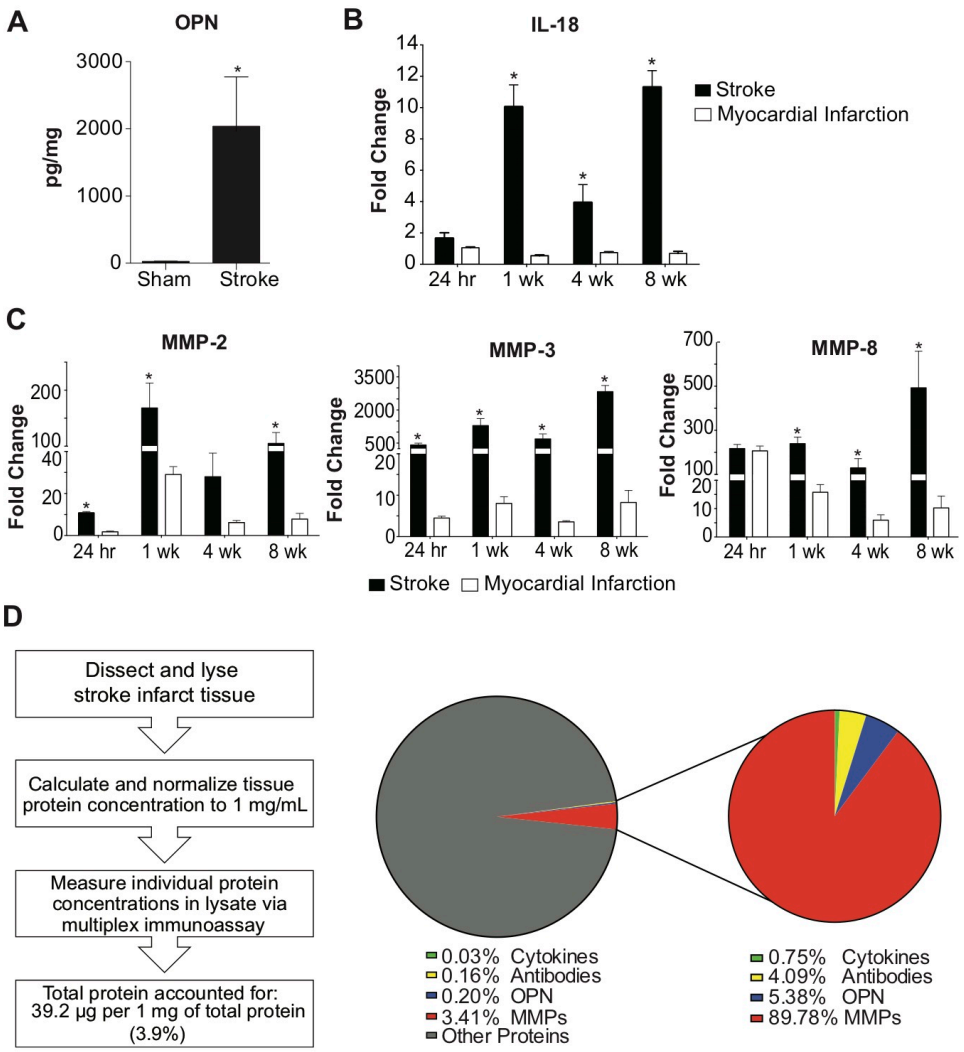

Fig. 3. Liquefaction of the brain following stroke shares multiple characteristics with atherosclerosis. (**A**) There is a significant elevation of OPN in the area of liquefactive necrosis at 7 weeks following stroke compared to the equivalent area in the cortex from sham mice. Data represent mean ± SEM from n=6 mice per experimental group. (**B**) There is significant elevation of IL-18 in the brain infarct at 1 week, 4 weeks, and 8 weeks following ischemic injury compared to the heart infarct. A biphasic elevation of IL-18 is seen in brain infarcts which peaks at 1 week and 8 weeks following stroke. Fold change compared to naïve tissue controls. (**C**) MMP-2 levels are significantly elevated within the brain infarct at 24 hours, 1 week, and 8 weeks following

ischemic injury compared to the heart infarct. MMP-3 levels are significantly elevated within the brain infarct at 24 hours, 1 week, 4 weeks, and 8 weeks following ischemic injury compared to the heart infarct. MMP-8 levels are significantly elevated within the brain infarct at 1 week, 4 weeks, and 8 weeks following ischemic injury compared to the heart infarct. Fold change compared to naïve tissue controls. *$p<0.05$. (**D**) Pie chart illustrating the relative percentage of total identified protein, cytokines, antibodies, OPN, and MMPs in 1mg of liquefactive necrosis. Antibody concentrations were taken from our previously published work [16] (**E**) Pie chart illustrating the dominance of MMP expression, by percentage, amongst the inflammatory molecules we have measured in areas of liquefactive necrosis. (3A-C courtesy of Jennifer Frye, 3D pie charts courtesy of Kristian P. Doyle).

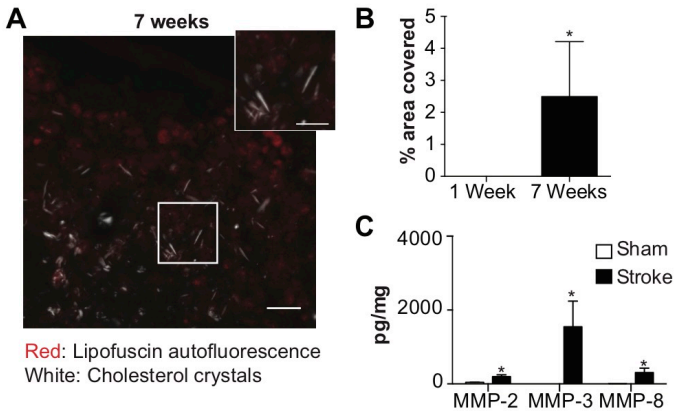

Fig. 4. Cholesterol crystals and MMPs also accumulate in the area of liquefactive necrosis following stroke in BALB/c mice. (**A**) Cholesterol crystals present in the infarct (delineated) at 7 weeks following stroke, visualized by overalaying images taken with polarized and fluorescent microscopy. Lipofuscin autofluorescence (red) denotes the lesion. Scale bar, 50 μm. Inset scale bar, 25 μm. (**B**) Cholesterol crystals appear in the infarct between 1 week and 7 weeks following stroke. (C) Levels of MMP-2, MMP-3, and MMP-4 are significantly in the infarct of stroked BALB/c mice compared to an equivalent area of the cortex in sham mice. *$p<0.05$. (4A-C courtesy of Megan Hayes).

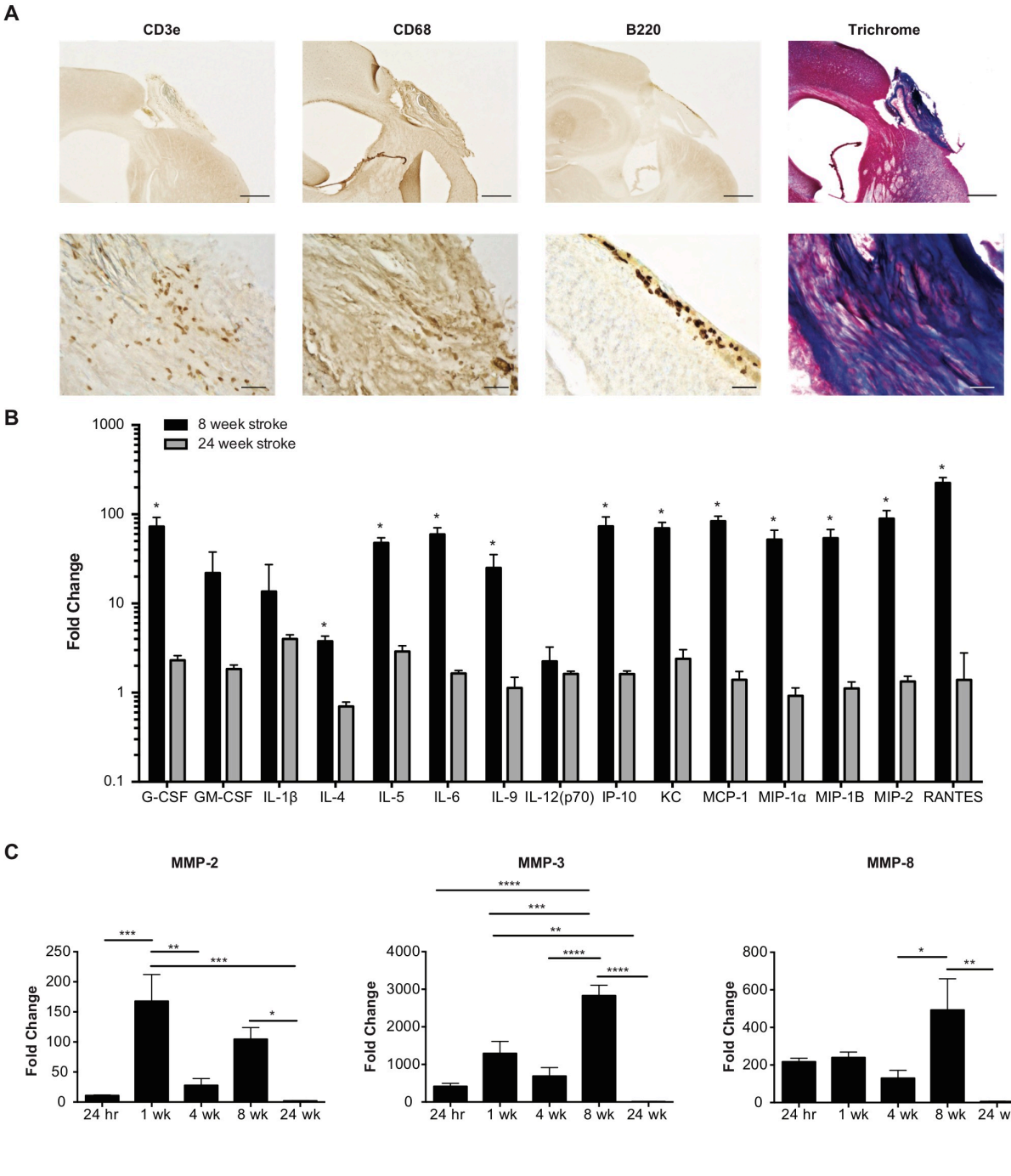

Fig. 5. Liquefactive necrosis subsides and a collagen scar is formed at 24 weeks following stroke in C57BL/6 mice. (**A**) Top panels show representative images of immune cell infiltration and collagen deposition in brain infarcts at 24 weeks post-stroke. Scale bar, 500 μm. Bottom panels show higher magnification images. Scale bar, 50 μm. There is a decrease in the

number of T-lymphocytes (CD3e; left panel), microglia/macrophages (CD68; first middle panel), and B-lymphocytes (B220; second middle panel) in the infarct 24 weeks following stroke compared to 8 weeks. There is also a marked increase in collagen (Trichrome; blue) staining at 24 weeks following stroke compared to 8 weeks. (**B**) Multiplex immunoassays demonstrate a concomitant decrease in cytokines/chemokines within the infarct at 24 weeks following stroke compared to 8 weeks following stroke. (**C**) Multiplex immunoassays indicate that MMP levels within the infarct have also returned to baseline levels at 24 weeks following stroke. Data represents mean ± SEM from n=5-6 mice per experimental group. Fold change compared to naïve tissue controls. *$p<0.05$, **$p<0.01$, ***$p<0.001$, and ****$p<0.0001$. (5A-C courtesy of Jennifer Frye).

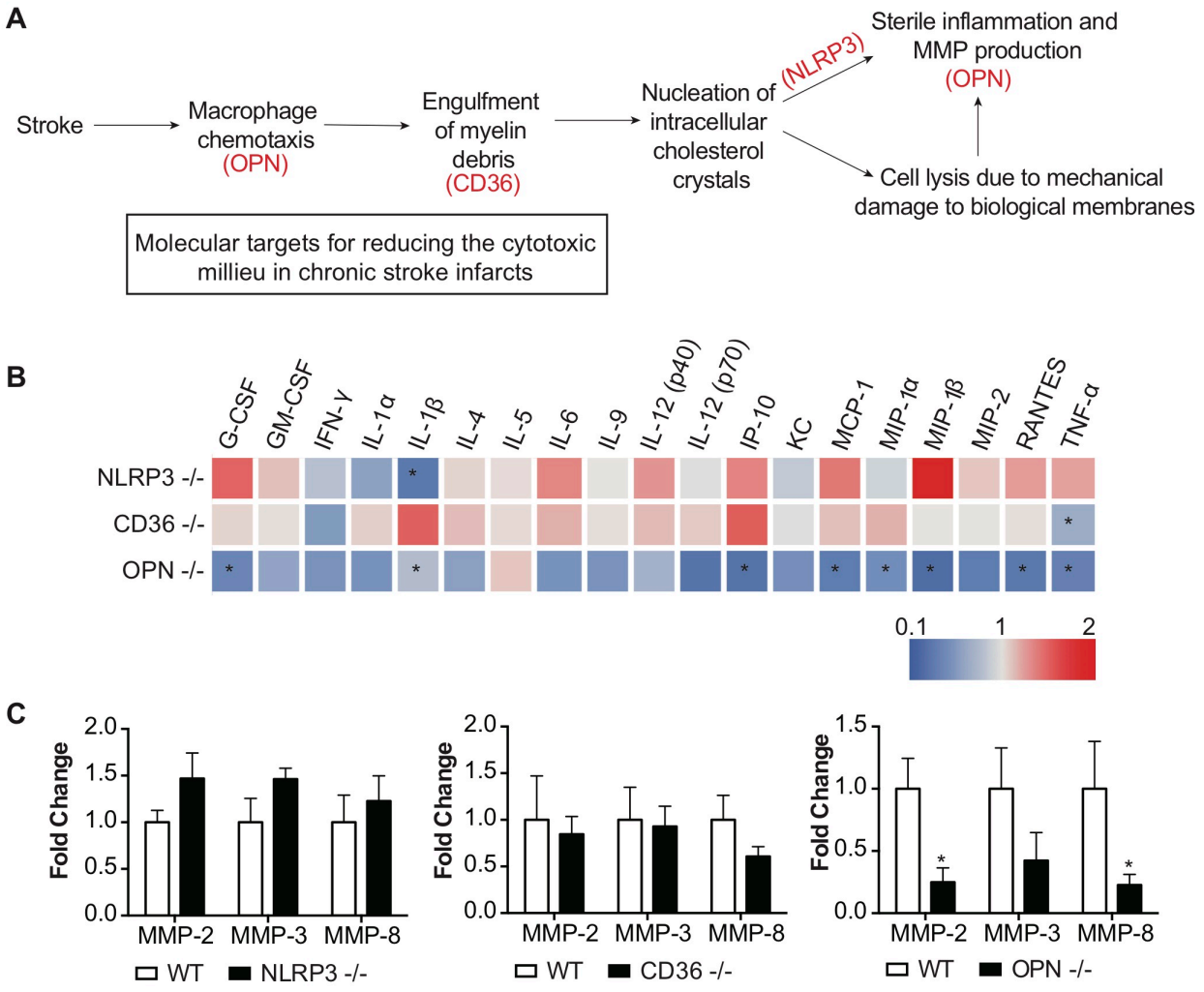

Fig. 6. Molecular targets for reducing the cytotoxic milieu in chronic stroke infarcts. (**A**) Rationale for targeting OPN, CD36, and NLRP3 as a means of curtailing the inflammatory response in areas of liquefactive necrosis following stroke. (**B**) Heat map of inflammatory marker levels in infarcted brain obtained by multiplex immunoassays demonstrates that the chronic inflammatory response was attenuated the most in OPN -/- mice. NLRP3 -/- mice showed a significant reduction in the chronic levels of IL-1β. CD36 -/- mice only showed a significant reduction in chronic levels of TNF-α. Data represents mean from n=6 mice per experimental group. (**C**) Multiplex immunoassays of MMPs show no significant changes in MMP levels in the chronic infarcts of NLRP3 -/- (left graph) and CD36 -/- (middle graph) mice

compared to wildtype mice. MMP levels are significantly and substantially lower in the chronic infarct of OPN -/- (right graph) mice when compared to wildtype. Data represents mean ± SEM from n=6 mice per experimental group. *$p<0.05$. (6A provided by Kristian P. Doyle, 6B-C courtesy of Jennifer Frye).

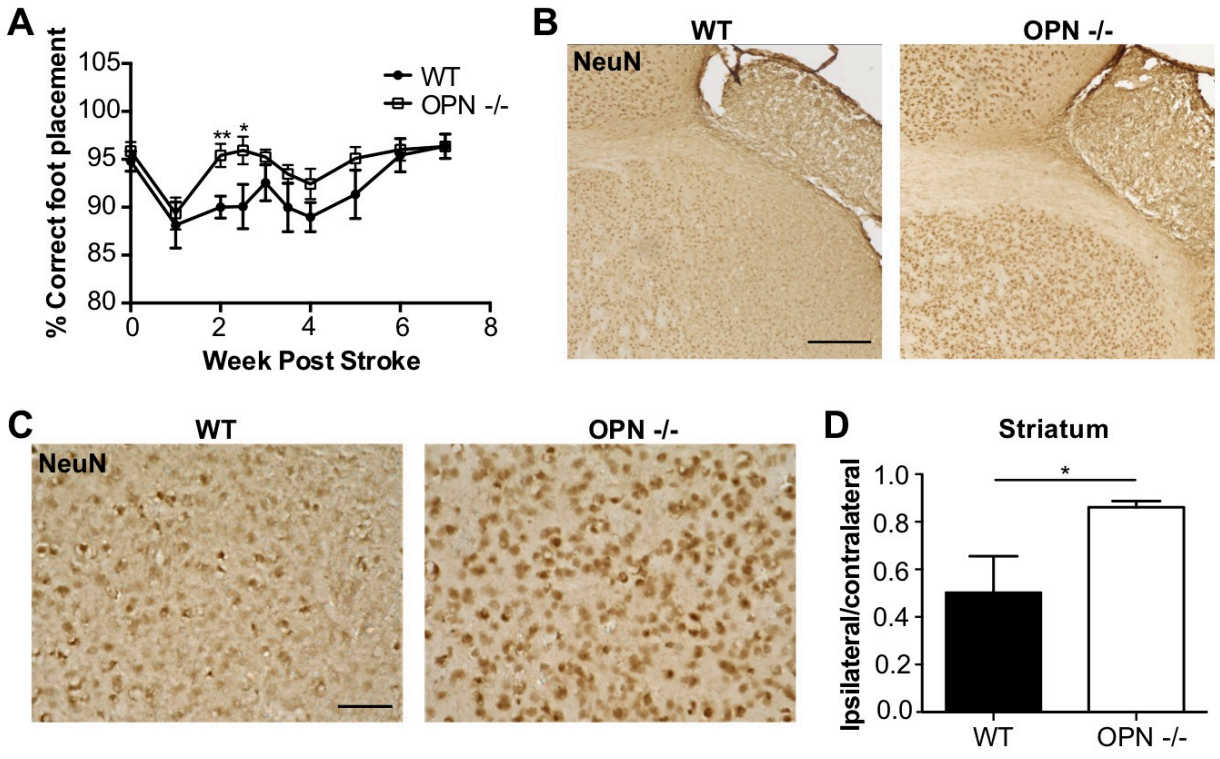

Fig. 7: Genetic ablation of OPN improves recovery and reduces secondary neurodegeneration following stroke. (**A**) Ladder rung tests were scored twice per week for the first 4 weeks following stroke and weekly thereafter. OPN -/- mice were able to recover faster on the ladder rung test compared to wildtype mice. *p<0.05 and **p<0.01 (**B**) Representative images showing preservation of NeuN immunoreactivity in chronic peri-infarct striatum of OPN -/- mice compared to wt mice. Scale bar, 250 μm. (**C**) Representative images showing preservation of NeuN immunoreactivity in chronic peri-infarct striatum of OPN -/- mice. Scale bar, 50 μm. (**D**) Quantitation of NeuN immunoreactivity in the peri-infarct striatum shows a significant increase in OPN -/- mice. Data represents mean ± SEM. *p<0.05. (7A courtesy of Jacob Zbesko).

REFERENCES

1. Benjamin EJ, Blaha MJ, Chiuve SE, et al. Heart Disease and Stroke Statistics—2017 Update: A Report From the American Heart Association. *Circulation*. January 2017:CIR.0000000000000485. doi:10.1161/CIR.0000000000000485

2. Béjot Y, Aboa-Eboulé C, Durier J, et al. Prevalence of early dementia after first-ever stroke: a 24-year population-based study. *Stroke*. 2011;42(3):607-612. doi:10.1161/STROKEAHA.110.595553

3. Leys D, Hénon H, Mackowiak-Cordoliani M-A, Pasquier F. Poststroke dementia. *Lancet Neurol*. 2005;4(11):752-759. doi:10.1016/S1474-4422(05)70221-0

4. González RG, Hirsch JA, Koroshetz WJ, Lev MH, Schaefer PW. *Acute Ischemic Stroke - Imaging and Intervention*.; 2006. http://www.springer.com/us/book/9783642127502. Accessed February 12, 2018.

5. Lee J-M, Grabb MC, Zipfel GJ, Choi DW. Brain tissue responses to ischemia. *J Clin Invest*. 2000;106(6):723-731. doi:10.1172/JCI11003

6. Aronowski J, Zhao X. Molecular pathophysiology of cerebral hemorrhage: Secondary brain injury. *Stroke J Cereb Circ*. 2011;42(6):1781-1786. doi:10.1161/STROKEAHA.110.596718

7. Kumar V, Abbas A, Aster J. *Robbins & Cotran Pathologic Basis of Disease - 9th Edition*. 9th ed.; 2014. https://www.elsevier.com/books/robbins-and-cotran-pathologic-basis-of-disease/kumar/978-1-4557-2613-4. Accessed February 12, 2018.

8. Zhang Q, Raoof M, Chen Y, et al. Circulating mitochondrial DAMPs cause inflammatory responses to injury. *Nature*. 2010;464:104-107.

9. Kerr JFR. A histochemical study of hypertrophy and ischaemic injury of rat liver with special reference to changes in lysosomes. *J Pathol Bacteriol*. 1965;90(2):419-435. doi:10.1002/path.1700900210

10. Kerr JFR, Wyllie AH, Currie AR. Apoptosis: A Basic Biological Phenomenon with Wide-ranging Implications in Tissue Kinetics. *Br J Cancer*. 1972;26(4):239-257.

11. Broughton BRS, Reutens DC, Sobey CG. Apoptotic mechanisms after cerebral ischemia. *Stroke*. 2009;40(5):e331-339. doi:10.1161/STROKEAHA.108.531632

12. Shen H, Kreisel D, Goldstein DR. Processes of sterile inflammation. *J Immunol Baltim Md 1950*. 2013;191(6):2857-2863. doi:10.4049/jimmunol.1301539

13. Huang J, Upadhyay UM, Tamargo RJ. Inflammation in stroke and focal cerebral ischemia. *Surg Neurol*. 2006;66(3):232-245. doi:10.1016/j.surneu.2005.12.028

14. Doyle KP, Simon RP, Stenzel-Poore MP. Mechanisms of ischemic brain damage. *Neuropharmacology*. 2008;55(3):310-318. doi:10.1016/j.neuropharm.2008.01.005

15. Zbesko JC, Nguyen T-VV, Yang T, et al. Glial scars are permeable to the neurotoxic environment of chronic stroke infarcts. *Neurobiol Dis*. 2018;112:63-78. doi:10.1016/j.nbd.2018.01.007

16. Doyle KP, Quach LN, Solé M, et al. B-lymphocyte-mediated delayed cognitive impairment following stroke. *J Neurosci Off J Soc Neurosci*. 2015;35(5):2133-2145. doi:10.1523/JNEUROSCI.4098-14.2015

17. Nguyen T-VV, Frye JB, Zbesko JC, et al. Multiplex immunoassay characterization and species comparison of inflammation in acute and non-acute ischemic infarcts in human and mouse brain tissue. *Acta Neuropathol Commun*. 2016;4(1):100. doi:10.1186/s40478-016-0371-y

18. Duewell P, Kono H, Rayner KJ, et al. NLRP3 inflammasomes are required for atherogenesis and activated by cholesterol crystals. *Nature*. 2010;464(7293):1357-1361. doi:10.1038/nature08938

19. Abela GS, Aziz K. Cholesterol crystals cause mechanical damage to biological membranes: a proposed mechanism of plaque rupture and erosion leading to arterial thrombosis. *Clin Cardiol*. 2005;28(9):413-420.

20. Corr EM, Cunningham CC, Dunne A. Cholesterol crystals activate Syk and PI3 kinase in human macrophages and dendritic cells. *Atherosclerosis*. 2016;251:197-205. doi:10.1016/j.atherosclerosis.2016.06.035

21. Moore KJ, Sheedy FJ, Fisher EA. Macrophages in atherosclerosis: a dynamic balance. *Nat Rev Immunol*. 2013;13(10):709-721. doi:10.1038/nri3520

22. Bayliss OB. The giant cell in cholesterol resorption. *Br J Exp Pathol*. 1976;57(5):610-618.

23. Sheikh Z, Brooks PJ, Barzilay O, Fine N, Glogauer M. Macrophages, Foreign Body Giant Cells and Their Response to Implantable Biomaterials. *Mater Basel Switz*. 2015;8(9):5671-5701. doi:10.3390/ma8095269

24. Stewart CR, Stuart LM, Wilkinson K, et al. CD36 ligands promote sterile inflammation through assembly of a Toll-like receptor 4 and 6 heterodimer. *Nat Immunol*. 2010;11(2):155-161. doi:10.1038/ni.1836

25. Orth M, Bellosta S. Cholesterol: Its Regulation and Role in Central Nervous System Disorders. Cholesterol. doi:10.1155/2012/292598

26. Cantuti-Castelvetri L, Fitzner D, Bosch-Queralt M, et al. Defective cholesterol clearance limits remyelination in the aged central nervous system. *Science*. January 2018. doi:10.1126/science.aan4183

27. Zhu X, Owen JS, Wilson MD, et al. Macrophage ABCA1 reduces MyD88-dependent Toll-like receptor trafficking to lipid rafts by reduction of lipid raft cholesterol. *J Lipid Res*. 2010;51(11):3196-3206. doi:10.1194/jlr.M006486

28. O'Regan A, Berman JS. Osteopontin: a key cytokine in cell-mediated and granulomatous inflammation. *Int J Exp Pathol*. 2000;81(6):373-390. doi:10.1046/j.1365-2613.2000.00163.x

29. Scatena M, Liaw L, Giachelli CM. Osteopontin: a multifunctional molecule regulating chronic inflammation and vascular disease. *Arterioscler Thromb Vasc Biol*. 2007;27(11):2302-2309. doi:10.1161/ATVBAHA.107.144824

30. Bruemmer D, Collins AR, Noh G, et al. Angiotensin II–accelerated atherosclerosis and aneurysm formation is attenuated in osteopontin-deficient mice. *J Clin Invest*. 2003;112(9):1318-1331. doi:10.1172/JCI200318141

31. Park YM. CD36, a scavenger receptor implicated in atherosclerosis. *Exp Mol Med*. 2014;46(6):e99. doi:10.1038/emm.2014.38

32. Sheedy FJ, Grebe A, Rayner KJ, et al. CD36 coordinates NLRP3 inflammasome activation by facilitating intracellular nucleation of soluble ligands into particulate ligands in sterile inflammation. *Nat Immunol*. 2013;14(8):812-820. doi:10.1038/ni.2639

33. Doyle KP, Fathali N, Siddiqui MR, Buckwalter MS. Distal hypoxic stroke: A new mouse model of stroke with high throughput, low variability and a quantifiable functional deficit. *J Neurosci Methods*. 2012;207(1):31-40. doi:10.1016/j.jneumeth.2012.03.003

34. Pollak J, Doyle KP, Mamer L, Shamloo M, Buckwalter MS. Stratification substantially reduces behavioral variability in the hypoxic-ischemic stroke model. *Brain Behav*. 2012;2(5):698-706. doi:10.1002/brb3.77

35. Braunersreuther V, Mach F, Steffens S. The specific role of chemokines in atherosclerosis. *Thromb Haemost*. 2007;97(5):714-721.

36. Ramji DP, Davies TS. Cytokines in atherosclerosis: Key players in all stages of disease and promising therapeutic targets. *Cytokine Growth Factor Rev*. 2015;26(6):673-685. doi:10.1016/j.cytogfr.2015.04.003

37. Adigun R, Bhimji SS. Necrosis, Cell (Liquefactive, Coagulative, Caseous, Fat, Fibrinoid, and Gangrenous). In: *StatPearls*. Treasure Island (FL): StatPearls Publishing; 2017. http://www.ncbi.nlm.nih.gov/books/NBK430935/. Accessed February 12, 2018.

38. Kashiwagi M, Liu L, Chu KK, et al. Feasibility of the assessment of cholesterol crystals in human macrophages using micro optical coherence tomography. *PloS One*. 2014;9(7):e102669. doi:10.1371/journal.pone.0102669

39. Tangirala RK, Jerome WG, Jones NL, et al. Formation of cholesterol monohydrate crystals in macrophage-derived foam cells. *J Lipid Res*. 1994;35(1):93-104.

40. Khan SR, Johnson JM, Peck AB, Cornelius JG, Glenton PA. Expression of osteopontin in rat kidneys: induction during ethylene glycol induced calcium oxalate nephrolithiasis. *J Urol*. 2002;168(3):1173-1181. doi:10.1097/01.ju.0000024398.45396.6c

41. Tenger C, Sundborger A, Jawien J, Zhou X. IL-18 accelerates atherosclerosis accompanied by elevation of IFN-gamma and CXCL16 expression independently of T cells. *Arterioscler Thromb Vasc Biol*. 2005;25(4):791-796. doi:10.1161/01.ATV.0000153516.02782.65

42. Singh RB, Mengi SA, Xu Y-J, Arneja AS, Dhalla NS. Pathogenesis of atherosclerosis: A multifactorial process. *Exp Clin Cardiol*. 2002;7(1):40-53.

43. Lund SA, Wilson CL, Raines EW, Tang J, Giachelli CM, Scatena M. Osteopontin mediates macrophage chemotaxis via α4 and α9 integrins and survival via the α4 integrin. *J Cell Biochem*. 2013;114(5):1194-1202. doi:10.1002/jcb.24462

44. Mi Z, Oliver T, Guo H, Gao C, Kuo PC. Thrombin-Cleaved COOH-Terminal Osteopontin Peptide Binds with Cyclophilin C to CD147 in Murine Breast Cancer Cells. *Cancer Res*. 2007;67(9):4088-4097.

45. Gu L, Okada Y, Clinton SK, et al. Absence of Monocyte Chemoattractant Protein-1 Reduces Atherosclerosis in Low Density Lipoprotein Receptor–Deficient Mice. *Mol Cell*. 1998;2(2):275-281. doi:10.1016/S1097-2765(00)80139-2

46. Dufour JH, Dziejman M, Liu MT, Leung JH, Lane TE, Luster AD. IFN-γ-Inducible Protein 10 (IP-10; CXCL10)-Deficient Mice Reveal a Role for IP-10 in Effector T Cell Generation and Trafficking. *J Immunol*. 2002;168(7):3195-3204. doi:10.4049/jimmunol.168.7.3195

47. Niki T, Soeki T, Yamaguchi K, et al. Elevated Concentration of Interferon-Inducible Protein of 10 kD (IP-10) Is Associated With Coronary Atherosclerosis. *Int Heart J*. 2015;56(3):269-272. doi:10.1536/ihj.14-300

48. Veillard NR, Kwak B, Pelli G, et al. Antagonism of RANTES receptors reduces atherosclerotic plaque formation in mice. *Circ Res*. 2004;94(2):253-261. doi:10.1161/01.RES.0000109793.17591.4E

49. Chen Y, Popko B. Cholesterol crystals impede nerve repair. *Science*. 2018;359(6376):635-636.

50. Miron VE, Boyd A, Zhao J-W, et al. M2 microglia and macrophages drive oligodendrocyte differentiation during CNS remyelination. *Nat Neurosci*. 2013;16(9):1211-1218. doi:10.1038/nn.3469

51. Poli G, Biasi F, Leonarduzzi G. Oxysterols in the pathogenesis of major chronic diseases. *Redox Biol*. 2013;1(1):125-130. doi:10.1016/j.redox.2012.12.001

52. Wolak T. Osteopontin - a multi-modal marker and mediator in atherosclerotic vascular disease. *Atherosclerosis*. 2014;236(2):327-337. doi:10.1016/j.atherosclerosis.2014.07.004

53. Kahles F, Findeisen HM, Bruemmer D. Osteopontin: A novel regulator at the cross roads of inflammation, obesity and diabetes. *Mol Metab*. 2014;3(4):384-393. doi:10.1016/j.molmet.2014.03.004

54. Alexander CM, Werb Z. Proteinases and extracellular matrix remodeling. *Curr Opin Cell Biol*. 1989;1(5):974-982.

55. Könnecke H, Bechmann I. The role of microglia and matrix metalloproteinases involvement in neuroinflammation and gliomas. *Clin Dev Immunol*. 2013;2013:914104. doi:10.1155/2013/914104

56. Sternlicht MD, Werb Z. HOW MATRIX METALLOPROTEINASES REGULATE CELL BEHAVIOR. *Annu Rev Cell Dev Biol*. 2001;17:463-516. doi:10.1146/annurev.cellbio.17.1.463

57. Chandler S, Coates R, Gearing A, Lury J, Wells G, Bone E. Matrix metalloproteinases degrade myelin basic protein. *Neurosci Lett*. 1995;201(3):223-226.

58. D'Souza CA, Mak B, Moscarello MA. The Up-regulation of Stromelysin-1 (MMP-3) in a Spontaneously Demyelinating Transgenic Mouse Precedes Onset of Disease. *J Biol Chem*. 2002;277(16):13589-13596. doi:10.1074/jbc.M108817200

59. Fujimoto M, Takagi Y, Aoki T, et al. Tissue inhibitor of metalloproteinases protect blood-brain barrier disruption in focal cerebral ischemia. *J Cereb Blood Flow Metab Off J Int Soc Cereb Blood Flow Metab*. 2008;28(10):1674-1685. doi:10.1038/jcbfm.2008.59

60. Mroczko B, Groblewska M, Barcikowska M. The role of matrix metalloproteinases and tissue inhibitors of metalloproteinases in the pathophysiology of neurodegeneration: a literature study. *J Alzheimers Dis JAD*. 2013;37(2):273-283. doi:10.3233/JAD-130647

61. Zhang K, McQuibban GA, Silva C, et al. HIV-induced metalloproteinase processing of the chemokine stromal cell derived factor-1 causes neurodegeneration. *Nat Neurosci*. 2003;6(10):1064-1071. doi:10.1038/nn1127

62. Anderson JM, Rodriguez A, Chang DT. Foreign body reaction to biomaterials. *Semin Immunol*. 2008;20(2):86-100. doi:10.1016/j.smim.2007.11.004

63. McNally AK, MacEwan SR, Anderson JM. FOREIGN BODY-TYPE MULTINUCLEATED GIANT CELL FORMATION REQUIRES PROTEIN KINASE C β, δ, and ζ. *Exp Mol Pathol*. 2008;84(1):37-45. doi:10.1016/j.yexmp.2007.10.005

64. Agrawal SM, Yong VW. The many faces of EMMPRIN - roles in neuroinflammation. *Biochim Biophys Acta*. 2011;1812(2):213-219. doi:10.1016/j.bbadis.2010.07.018

65. Kong W, Li S, Longaker MT, Lorenz HP. Cyclophilin C-associated protein is up-regulated during wound healing. *J Cell Physiol*. 2007;210(1):153-160. doi:10.1002/jcp.20830

66. Yamaguchi R, Hosaka M, Torii S, et al. Cyclophilin C-associated protein regulation of phagocytic functions via NFAT activation in macrophages. *Brain Res*. 2011;1397:55-65. doi:10.1016/j.brainres.2011.03.036

67. Lindsey ML, Zouein FA, Tian Y, Padmanabhan Iyer R, de Castro Brás LE. Osteopontin is proteolytically processed by matrix metalloproteinase 9. *Can J Physiol Pharmacol*. 2015;93(10):879-886. doi:10.1139/cjpp-2015-0019

68. Malik AF, Hoque R, Ouyang X, et al. Inflammasome components Asc and caspase-1 mediate biomaterial-induced inflammation and foreign body response. *Proc Natl Acad Sci U S A*. 2011;108(50):20095-20100. doi:10.1073/pnas.1105152108

69. Gargiulo S, Sottero B, Gamba P, Chiarpotto E, Poli G, Leonarduzzi G. Plaque oxysterols induce unbalanced up-regulation of matrix metalloproteinase-9 in macrophagic cells through redox-sensitive signaling pathways: Implications regarding the vulnerability of atherosclerotic lesions. *Free Radic Biol Med*. 2011;51(4):844-855. doi:10.1016/j.freeradbiomed.2011.05.030

70. Miklossy J, Clarke S, Van der Loos H. The long distance effects of brain lesions: visualization of axonal pathways and their terminations in the human brain by the Nauta method. *J Neuropathol Exp Neurol*. 1991;50(5):595-614.

71. Miklossy J, Van der Loos H. Cholesterol ester crystals in polarized light show pathways in the human brain. *Brain Res*. 1987;426(2):377-380. doi:10.1016/0006-8993(87)90892-4

72. Smith ME. Phagocytosis of myelin in demyelinative disease: a review. *Neurochem Res*. 1999;24(2):261-268.

73. Coisne C, Tilloy S, Monflier E, Wils D, Fenart L, Gosselet F. Cyclodextrins as Emerging Therapeutic Tools in the Treatment of Cholesterol-Associated Vascular and Neurodegenerative Diseases. *Mol Basel Switz*. 2016;21(12). doi:10.3390/molecules21121748

74. Zimmer S, Grebe A, Bakke SS, et al. Cyclodextrin promotes atherosclerosis regression via macrophage reprogramming. *Sci Transl Med*. 2016;8(333):333ra50. doi:10.1126/scitranslmed.aad6100

75. Schmitt S, Castelvetri LC, Simons M. Metabolism and functions of lipids in myelin. *Biochim Biophys Acta*. 2015;1851(8):999-1005. doi:10.1016/j.bbalip.2014.12.016